

# Characterization of alumina and hafnia grown by low-temperature ALD

Molly P. Andersen<sup>1,2</sup> and Ilan T. Rosen<sup>3,2</sup>

<sup>1</sup>*Department of Materials Science, Stanford University, Stanford, California 94305, USA*

<sup>2</sup>*Stanford Institute for Materials and Energy Sciences,*

*SLAC National Accelerator Laboratory, Menlo Park, California 94025, USA*

<sup>3</sup>*Department of Applied Physics, Stanford University, Stanford, California 94305, USA*

(Dated: March 2020)

## INTRODUCTION

### Atomic layer deposition

Atomic layer deposition (ALD) is a type of chemical vapor deposition rapidly growing in popularity because it produces stoichiometric films of precise thickness, even on surfaces with highly irregular topography. ALD uses cycles of two or more self-limiting reactions, so that in principle, exactly one layer of the desired film is deposited each cycle.

A typical ALD process, shown schematically in Fig. 1, proceeds as follows. The substrate is placed inside a heated reactor, and the reactor is evacuated to low vacuum with a constant gas flow, typically of  $N_2$ . Precursor A is introduced into the chamber by exposing the reservoir of precursor to the chamber for a given pulse time (typically  $< 1$  s). Precursor A reacts with the substrate, leaving a monolayer of film component A on its surface. Residual precursor, along with reaction byproducts, are pumped out of the chamber for a given purge time. Precursor B is then introduced into the chamber, where it reacts with the monolayer of film component A, leaving a monolayer of film component B. The chamber is evacuated in the same way. This completes one ALD cycle; by repetition, alternating layers of film components A and B are accumulated. Optionally, when a precursor is introduced to the chamber, the chamber exhaust can be closed to hold the precursor in the reactor for a given exposure time, allowing the precursor more time to react with the sample.

### ALD at low temperatures

During ALD deposition, the substrate is typically to around  $200^\circ\text{C}$  in order to volatilize the precursor compounds and optimize the kinetics of the self-limiting reactions. Increasing interest, however, is developing around using ALD deposition with substrates that are incompatible with such high temperatures. In particular, we are interested in using V-VI-class topological insulators, such as  $\text{Bi}_2\text{Te}_3$ . These materials suffer from thermal damage at temperatures exceeding  $100^\circ\text{C}$  and we aim to process them at the lowest temperatures possible. Beyond our use case, a low-temperature ALD process enables depo-

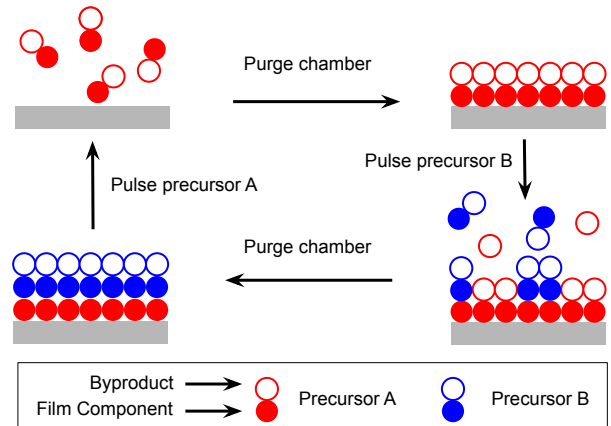


FIG. 1. Schematic of an ALD cycle. During the first cycle, the grey box would represent the substrate. During subsequent cycles, the grey box would represent the substrate plus the film accumulated from completed cycles

sition on transition metal dichalcogenides (e.g.  $\text{MoSe}_2$ ), polymer substrates (e.g. polydimethylsiloxane), biological substrates (e.g. lipid membranes), substrates patterned with photoresists or electron beam resists, and so on.

Specific problems may arise during a low temperature ALD process, which can cause the film growth rate to be either too high or too low. First, precursor volatility decreases at lower temperatures, so the precursor may condense or even fail to enter the reaction chamber. Second, reaction kinetics slow at lower temperatures, so the grown film may poorly wet the substrate, causing delayed or uneven film nucleation. Third, the precursor may not fully decompose, and additional atoms will be incorporated into the film. In particular, when using organometallic precursors, this results in carbon contamination. Fourth, precursor decomposition byproduct volatility decreases, and these byproducts may not be fully evacuated from the chamber during the purge step.

## METHODS

### Film growth

In this work, we concentrate on the growth of films of alumina ( $\text{AlO}_x$ ) and hafnia ( $\text{HfO}_2$ ) at  $60^\circ\text{C}$  and  $85^\circ\text{C}$ , respectively. Amorphous alumina can be grown even at room temperature, as the organometallic Al precursor trimethylaluminum (TMA) is extremely volatile. Although no crystallinity is expected to result from low temperature growth driven by thermal energy alone, crystalline aluminum oxide ( $\text{Al}_2\text{O}_3$ ) can be grown with high temperature plasma enhanced ALD, which is beyond the scope of this work. The Hf precursor tetrakis(dimethylamido)hafnium (TDMA-Hf) must be heated to  $75^\circ\text{C}$  to be volatile; to ensure an appropriate thermal gradient across the ALD reactor, the minimum substrate temperature for hafnium growth is  $85^\circ\text{C}$ . Crystalline hafnium oxide ( $\text{HfO}_2$ ) is difficult to achieve through ALD without aggressive post-growth annealing. Water ( $\text{H}_2\text{O}$ ) was used as the oxygen precursor for both alumina and hafnia films.

In this work, all films were grown in a Savannah S200 thermal ALD system (Cambridge NanoTech). During growth, 20 sccm  $\text{N}_2$  was flowed through the reactor, resulting in base pressure of roughly  $2e-1$  Torr. After opening the reactor to insert a sample, the reactor was pumped for 15 minutes prior to every growth to evacuate water out of the reactor. Except where otherwise noted, alumina films were grown at  $60^\circ\text{C}$  using 60 s purge times for both TMA precursor and water. Except where otherwise noted, hafnia films were grown at  $85^\circ\text{C}$  using a 5 s exposure step, a 40 s purge time for TDMA-Hf precursor, and a 60 s purge time for water.

In some cases, a seed layer was deposited prior to ALD growth using an electron beam evaporator (Kurt J. Lesker). For alumina films, aluminum was deposited in steps of 1 nm, allowing the film to oxidize in air for 20 min between steps. For hafnia films, hafnium was deposited in steps of 0.6 nm, similarly oxidizing between steps. Substrates were cleaned using organic solvents before seed growth as well as before ALD growth.

### Film characterization

In this work, we primarily focus on the growth of thick ( $> 5$  nm) oxide films for use as gate dielectrics. The crucial film quality metrics for gate dielectrics are dielectric constant and breakdown field. The product of these two figures is proportional to the maximum carrier accumulation/depletion that the gate oxide may provide. We assessed these metrics by fabricating and measuring metal-insulator-metal (MIM) capacitors, where the metal is platinum and the insulator is the oxide film. Platinum, a noble metal, was chosen to prevent an un-

wanted oxide layer forming on the bottom metal contact prior to ALD oxide growth. The bottom contact and dielectric layers were deposited uniformly by electron beam evaporation and ALD, respectively, and the top contact was deposited by electron beam evaporation with a shadow mask to form circular MIM devices of diameter  $d = 100 \mu\text{m}$ . Capacitance  $C$  was measured at 1 kHz. The dielectric breakdown voltage  $V_b$  was determined by DC current-voltage measurement. As the applied voltage across the device is increased,  $V_b$  is determined as the voltage at which the current through the device increases discontinuously and irreversibly. Error bars represent the standard deviation of  $n = 3$  samples; all data points presented without error bars represent a single sample.

In addition, we performed structural and chemical characterization of the thick film oxides. Film thickness was measured by atomic force microscopy (AFM), supplemented by ellipsometry. To use AFM, ALD films were grown on  $\text{SiO}_2$  and  $(\text{Bi}_x\text{Sb}_{1-x})_2\text{Te}_3$  partially masked by polymethyl methacrylate (PMMA), after which a step was formed by lifting off the masked region by sonication in organic solvents. Ellipsometry was used to characterize films grown on  $\text{SiO}_2$ . Film composition was analyzed using x-ray photoelectron spectroscopy (XPS) and x-ray fluorescence (XRF).

The ALD reactor is sized to hold 200 mm round wafers. To characterize the uniformity of film growth throughout the reactor, we placed  $n = 5$   $\text{SiO}_2$  chips around the reactor. The chip locations were center, far left (near the precursor injection port), far right (near the exhaust port), top, and bottom. We measured the film thickness  $\{t_i\}$  using ellipsometry. As a metric of uniformity, we introduce the root-mean-square (RMS) nonuniformity:

$$u = \frac{1}{\bar{t}} \sqrt{\sum_{i=1}^n (t_i - \bar{t})^2} \quad (1)$$

where  $\bar{t} = \frac{1}{n} \sum_{i=1}^n t_i$  is the mean thickness. Despite containing information about only a single growth, we posit that the RMS nonuniformity may correlate with process repeatability.

## ALUMINA THICK FILMS

### Effect of Temperature

The rate of ALD alumina growth is only slightly sensitive to temperature. Between  $100^\circ\text{C}$  and  $60^\circ\text{C}$  reactor temperature, the film thickness decreased by 4% (Fig. 2). This result encourages that the low-temperature ALD process is stable and does not suffer from the previously mentioned issues that can plague low-temperature processes.

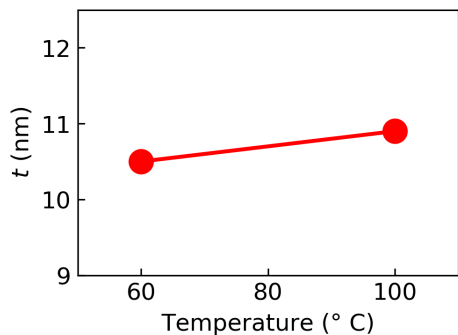


FIG. 2. Thickness of 100 cycle ALD alumina films versus reactor temperature

### Effect of Purge Times

The uniformity of ALD alumina growth is highly sensitive to the precursor purge times. Increasing the purge times for both TMA and water precursors from 25 s to 60 s decreased the RMS nonuniformity from 23% to 11% (Fig. 3). Furthermore, increasing the purge times to 60 s substantially improves the maximum gate swing of the dielectric, as shown in Fig. 4.

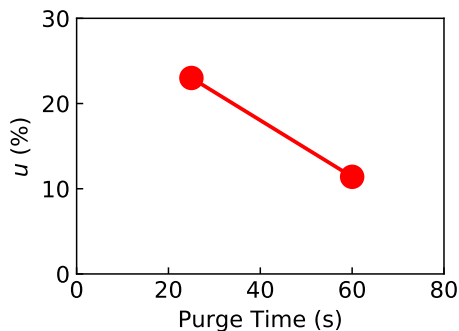


FIG. 3. RMS nonuniformity of ALD alumina films amongst a variety of locations in the reactor, versus the purge times of both precursors, TMA and water

### Film Composition

Deposition temperature can impact the ultimate composition of an ALD film. If precursors lack sufficient thermal energy to completely react with one another, extraneous components of one or both precursors may be incorporated into the film. For example, residual carbon from the organometallic precursor is often observed in low-temperature metal oxides [1, 2].

XPS was used to analyze the composition of 100 cycles of alumina deposited at both 60°C and 200°C; survey scans for both films are shown in Fig. A1. The ratios of carbon to aluminum to oxygen are identical to within

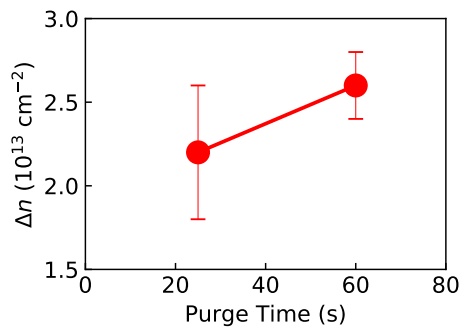


FIG. 4. Maximum gate swing of 100 cycle ALD alumina films versus the purge times of both precursors, TMA and water

2% between the two films, which is roughly the limit on precision of XPS quantitation. These results indicate no substantial compositional variations occur at low temperatures.

### Film Density

X-ray fluorescence was used to quantify aluminum content in 100 cycles of alumina deposited at 60°C, and in a reference film deposited at 200°C. The ratio of aluminum found in the 60°C film to aluminum in the 200°C film is 0.789:1. Since XPS characterization confirms that the fraction of aluminum in the films is not changing, this data suggests that the low-temperature film is less dense than the standard film.

### Linear Growth Rate

AFM was used to measure the thicknesses of 60, 100, and 140 cycles of low-temperature alumina deposited on SiO<sub>2</sub>. Data and a linear fit are shown in Fig. 5. The fit reveals a growth rate of 0.8 Å/cycle, which agrees well with the typical expectation of 1.0 Å/cycle for standard alumina depositions and could suggest high film quality [3]. However, the 0-cycle intercept of 2.1 nm indicates excess growth for the first few cycles, which is not typical in standard alumina films. While this could suggest that the initial cycles produce poor quality alumina, additional data is necessary to make any firm claims.

### Growth on Seeded Substrates

Al seed layers with as-grown thickness  $s_{\text{nom}} = 1, 2,$  and 3 nm (i.e., the total thickness of metal prior to oxidation) were deposited. The seed layers swell when oxidized in air. AFM measurements (Fig. 6) show that the thickness

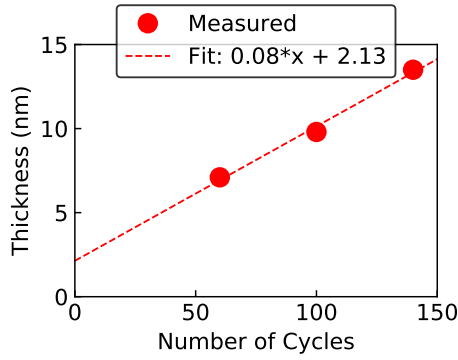


FIG. 5. Thickness of ALD alumina films grown with 60, 100, and 140 cycles. A linear fit (dashed line) demonstrates reveals the constant growth rate

of the oxidized films,  $s_{\text{meas}}$ , depends linearly on the as-grown thickness as  $s_{\text{meas}}/s_{\text{nom}} = 2.95$ .

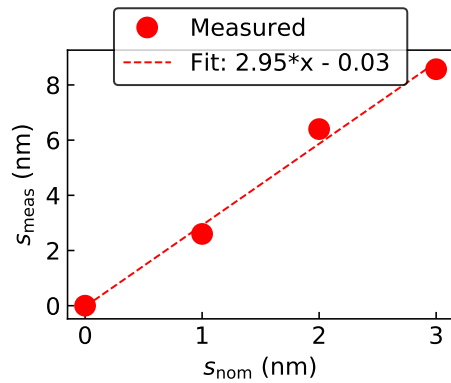


FIG. 6. Measured seed layer thickness  $s_{\text{meas}}$  versus as-grown thickness  $s_{\text{nom}}$  for Al seed layers

The thickness of 140 cycle ALD alumina films are shown in Fig. 7 for films grown on  $\text{SiO}_2$  and  $(\text{Bi}_x\text{Sb}_{1-x})_2\text{Te}_3$  (topological insulator, or TI) substrates with varying seed layer thicknesses. We observe no correlation between film thickness and seed layer thickness on  $\text{SiO}_2$  substrates. On  $(\text{Bi}_x\text{Sb}_{1-x})_2\text{Te}_3$ , the film grown with no seed layer was thicker than those grown on a seed layer.

### Electrical Properties

The dielectric breakdown field is defined as  $E_b = V_b/t$  where  $t$  is the thickness of the dielectric and  $V_b$  is the breakdown voltage of the device. The breakdown field of alumina films versus seed layer thickness is shown in Fig. 8 for various alumina thicknesses.

The relative dielectric constant of the devices were determined by measuring  $C$ , the capacitance of the MIM

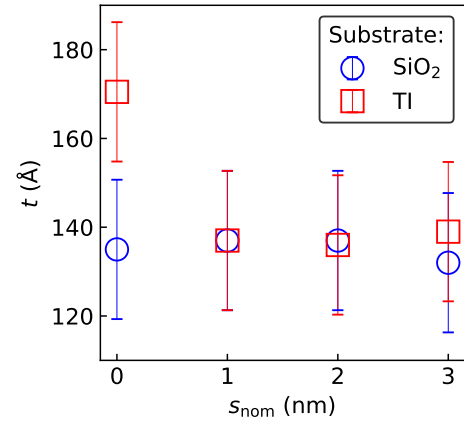


FIG. 7. Thickness of 140 cycles of ALD alumina versus as-grown seed layer thickness. The reported thickness of the ALD film does not include the thickness of the seed layer

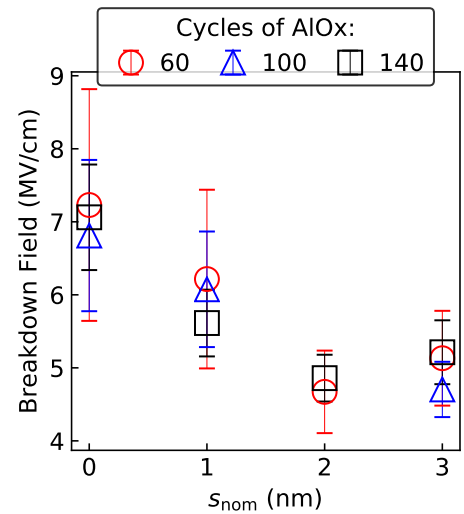


FIG. 8. Breakdown field of alumina films versus as-grown seed layer thickness, shown for 60, 100, and 140 cycle ALD films

devices at 1 kHz. The relative dielectric constant is given by  $\epsilon_r = tC/\epsilon_0A$  where  $\epsilon_0$  is the vacuum permittivity and the device area is  $A = \pi d^2/4$ . The relative dielectric constant of alumina films versus seed layer thickness is shown in Fig. 9 for various alumina thicknesses.

The maximum gate swing  $\Delta n$  of a dielectric represents the maximum carrier density that can be accumulated or depleted using an electrostatic gate made of the dielectric. The maximum gate swing is given by  $\Delta n = \epsilon_0\epsilon_r V_b$ . Unlike  $\epsilon_r$  and  $V_b$ ,  $\Delta n$  is determined without knowledge of  $t$ , thereby limiting a potential source of error. The maximum gate swing of alumina films versus seed layer thickness is shown in Fig. 10. We observe a negative correlation between  $t_s$  and  $\Delta n$ , indicating that unseeded ALD films form the best gate dielectrics. In addition, we

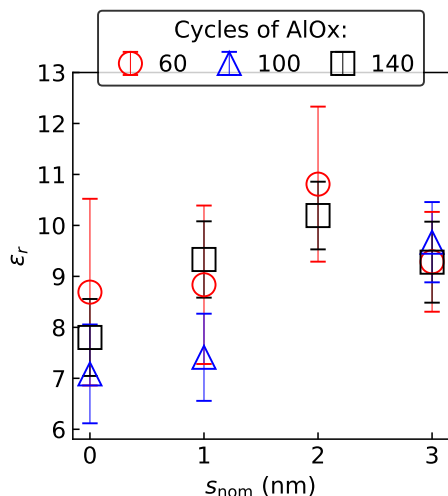


FIG. 9. Relative dielectric constant of alumina films versus as-grown seed layer thickness, shown for 60, 100, and 140 cycle ALD films

observed that  $\Delta n$  is higher for 60 cycle ALD films than 100 and 140 cycle films; we lack an explanation for this observation.

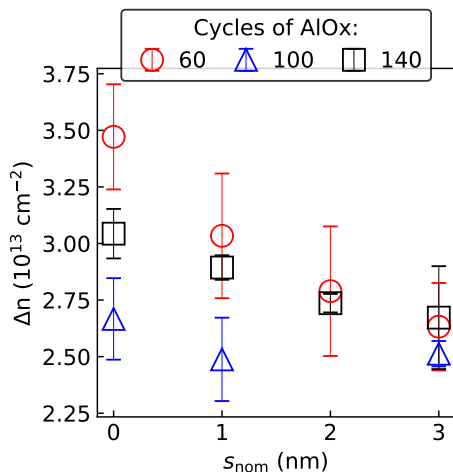


FIG. 10. Maximum gate swing of alumina films versus as-grown seed layer thickness, shown for 60, 100, and 140 cycle ALD films

## HAFNIA THICK FILMS

### Effect of Temperature

The rate of ALD hafnia growth is highly sensitive to temperature. Between 100°C and 85°C reactor temperature, the film thickness increased by 19% (Fig. 11). This finding indicates that ALD hafnia growth is not entirely

stable at 85° C. We proceed to show that films of useful quality may nevertheless be achieved.

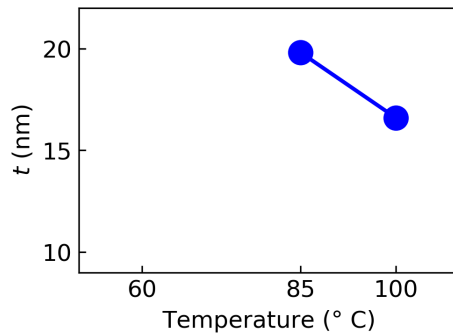


FIG. 11. Thickness of 100 cycle ALD hafnia films versus reactor temperature

### Effect of Purge Times

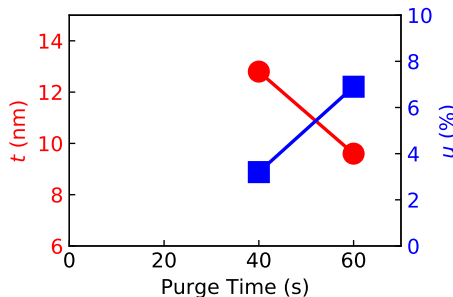


FIG. 12. Thickness (left axis) and RMS nonuniformity (right axis) of 100 cycle Hf films shown as a function of TDMA-Hf purge time. Purge times for water are 60 s

The impact of lengthening the TDMA-Hf purge time is shown in Fig. 12. The film grown with a longer purge time is thinner, while the RMS nonuniformity is higher with the longer purge time. This behavior may result from desorption of the TDMA-Hf precursor from the substrate during the 60 s purge time. These observations delineate the acceptable range of purge times: the lower limit is set by the need to pump out excess precursor, and the upper, by the need to retain as much adsorbed precursor as possible. Despite the change in growth rate, the maximum gate swing, shown in Fig. 13, varies minimally with the purge time.

### Effect of Exposure

One way to combat reduced precursor volatility at reduced temperatures is the introduction of an exposure step into each cycle of ALD. Before pulsing the precursor

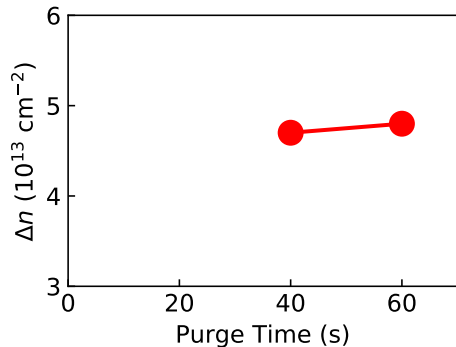


FIG. 13. Maximum gate swing of 100 cycle Hf films shown as a function of TDMA-Hf purge time. Purge times for water are 60 s

of interest, the deposition chamber is sealed from the exhaust line (to the vacuum pump). The precursor is then injected into the deposition chamber where it remains, allowing extra time for available sites on the substrate to react with the precursor. After this period of extra precursor exposure ends, the deposition chamber is opened to the exhaust line and the precursor is evacuated. We note that, during the exposure step, carrier gas ( $\text{N}_2$ ) flow must be reduced to avoid over-pressure of the deposition chamber.

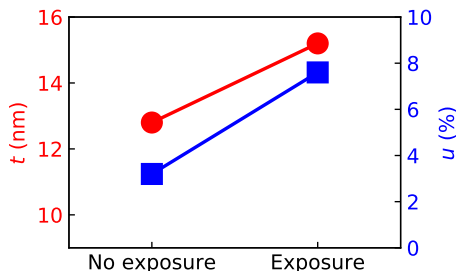


FIG. 14. Thickness (left axis) and RMS nonuniformity (right axis) of 100 cycle Hf films grown without and with 5 s exposure. Purge times are 40 s for TDMA-Hf and 60 s for water

The impact of adding an exposure step on the structural properties of Hf films is shown in Fig. 14. As expected, the film grown with exposure is thicker. The RMS nonuniformity is slightly higher with exposure; we lack an explanation for this observation but note that the RMS nonuniformity is low in both growths. The maximum gate swing, shown in Fig. 15, is minimally affected by the addition of an exposure step.

Fig. 16 shows AFM profiles of hafnia films grown with various purge time and exposure conditions. Steps in the films were created by drop-casting PMMA before film deposition, and lifting off afterwards. The AFM profiles were averaged over a few microns along the step edges (transverse to the  $x$  axis). The film grown with an ex-

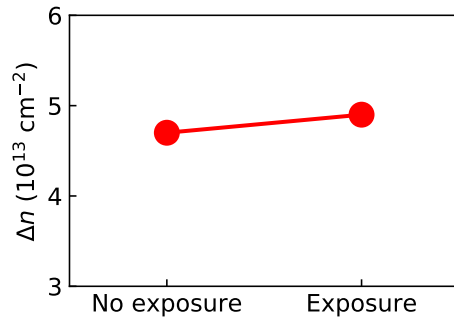


FIG. 15. Maximum gate swing of 100 cycle Hf films grown without and with 5 s exposure. Purge times are 40 s for TDMA-Hf and 60 s for water.

posure step had the smallest reduction in thickness near the step edge. This observation is consistent with the hypothesis that the exposure step allows the TDMA-Hf precursor to more completely saturate available sites on the substrate during each cycle, particularly near topographical or chemical changes in the substrate. Since the electrical properties of the dielectric were unchanged by the addition of the exposure step, we suggest using a 40 s purge time for TDMA-Hf precursor and including an exposure step in Hf films, particularly when grown on uneven substrates.

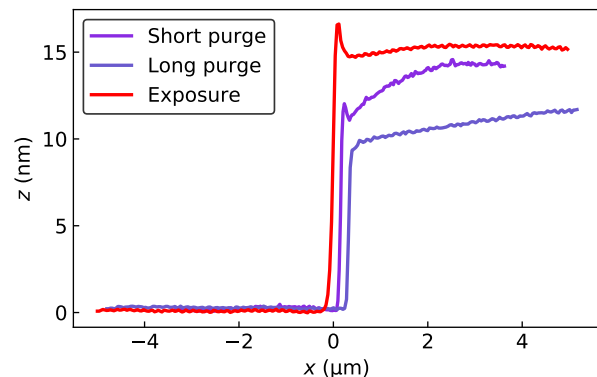


FIG. 16. Line cuts of AFM images taken across a step edge of hafnia ALD, created by lifting off a masked region after 100 cycles of ALD growth. Line cuts are shown for films grown with (purple) 40 s purge time, (blue) 60 s purge time, and (red) 5 s exposure and 40 s purge time for TDMA-Hf precursor. The purge time for water precursor was 60 s for all films

### Linear Growth Rate

AFM was used to measure the thicknesses of 60, 100, and 140 cycles of low-temperature hafnia deposited on  $\text{SiO}_2$ . Data are shown in Fig. 17. A linear fit reveals a growth per cycle of 2.0 Å, which exceeds that at higher

temperatures, 1.0 Å [3]. The elevated growth rate may be due to incomplete breakdown of the TDMA-Hf precursor molecule, and therefore incorporation of nitrogen and carbon in the film. Furthermore, the 0-cycle intercept of 1.3 nm indicates excess growth for the first few cycles.

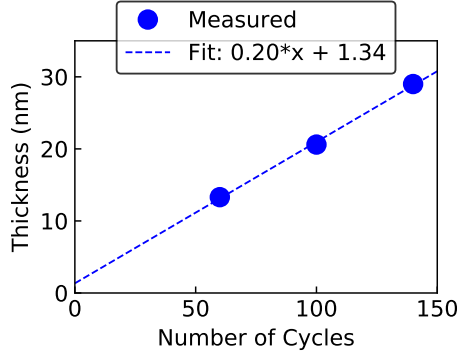


FIG. 17. Thickness of ALD hafnia films grown with 60, 100, and 140 cycles. A linear fit (dashed line) demonstrates the constant growth rate

#### Growth on Seeded Substrates

Hafnium metal was deposited to form seed layers with nominal thicknesses of 0, 0.6, 1.2, and 1.8 nm prior to oxidation. After oxidation, the Hf seed layers swell in thickness by the factor  $s_{\text{meas}}/s_{\text{nom}} = 2.1$  (Fig. 18).

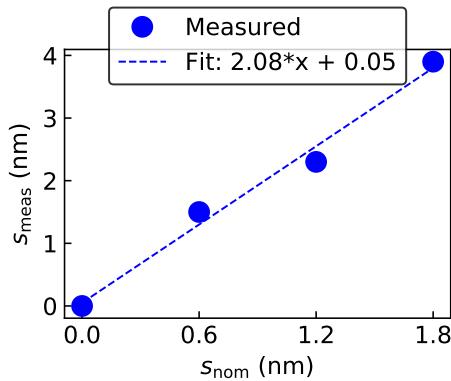


FIG. 18. Measured seed layer thickness  $s_{\text{meas}}$  versus as-grown thickness  $s_{\text{nom}}$  for Hf seed layers

The thickness of 140 cycle ALD hafnia films are shown in Fig. 19 for films grown on  $\text{SiO}_2$  and  $(\text{Bi}_x\text{Sb}_{1-x})_2\text{Te}_3$  substrates with varying seed layer thicknesses. We observe no substantial correlation between film thickness and seed layer thickness on either substrate.

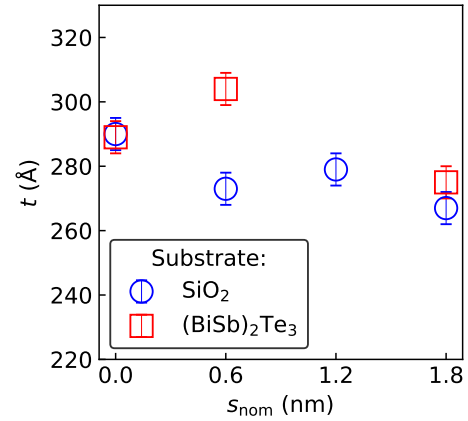


FIG. 19. Thickness of 140 cycles of ALD hafnia versus as-grown seed layer thickness. The reported thickness of the ALD film does not include the thickness of the seed layer

#### Electrical Properties

The breakdown field and relative dielectric constant of hafnia films versus seed layer thickness is shown in Fig. 20 and Fig. 21, respectively, for various hafnia thicknesses. Neither quantity correlates with seed thickness.

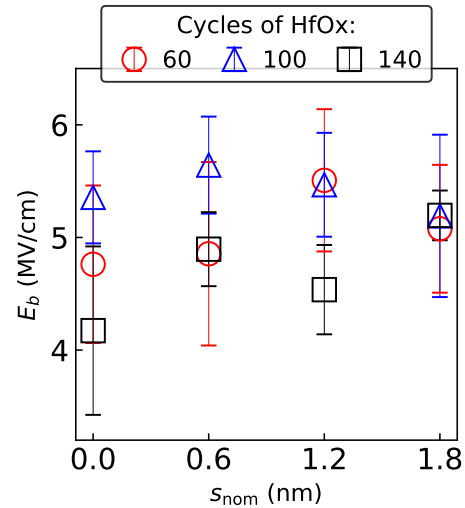


FIG. 20. Breakdown field of hafnia films versus as-grown seed layer thickness, shown for 60, 100, and 140 cycle ALD films

The maximum gate swing of hafnia films versus seed layer thickness is shown in Fig. 22. We observe that  $\Delta n$  correlates with neither  $t_s$  nor the film thickness. The maximum gate swing we achieve,  $\Delta n \approx 4.5e13 \text{ cm}^{-2}$ , is lower than what may be obtained from hafnia films grown at higher temperatures; nevertheless, this value eclipses that of alumina films despite the hafnium precursor's low volatility at low temperatures. However, it should be noted that, at room temperature, the leak-

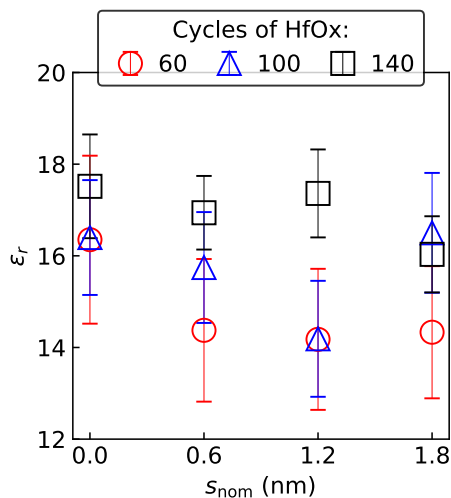


FIG. 21. Relative dielectric constant of hafnia films versus as-grown seed layer thickness, shown for 60, 100, and 140 cycle ALD films

age current through hafnia was substantially larger than that through alumina (data not shown due to COVID-19), and may surpass an acceptable limit far prior to the true dielectric breakdown used in these calculations.

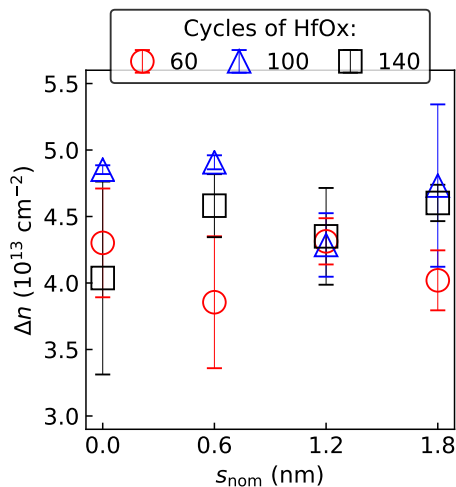


FIG. 22. Maximum gate swing of hafnia films versus as-grown seed layer thickness, shown for 60, 100, and 140 cycle ALD films

## CONCLUSION

We have demonstrated low-temperature ALD growth of alumina and hafnia films suitable for use as gate dielectrics. We produced alumina films with relative dielectric constant roughly equivalent to ALD films grown at high temperature ( $\epsilon_r \approx 9$ ) and hafnia films with rel-

ative dielectric constant about 65 % that of crystalline films ( $\epsilon_r \approx 16$  in our films versus  $\epsilon_r \approx 25$  in crystalline material)[4, 5].

- 
- [1] E. Ghiraldelli, C. Pelosi, E. Gombia, G. Chiavarotti, and L. Vanzetti, *Thin Solid Films* **517**, 434 (2008).
  - [2] C. Detavernier, J. Dendooven, D. Deduytshe, and J. Musschoot, *ECS Transactions* **16**, 239 (2008).
  - [3] "Snf savannah qualification data," <https://snfexfab.stanford.edu/snf/operating-instructions/savannah-in-depth>, accessed: 2020-03-24.
  - [4] G. D. Wilk, R. M. Wallace, and J. M. Anthony, *Journal of Applied Physics* **89**, 5243 (2001).
  - [5] J. Choi, Y. Mao, and J. Chang, *Materials Science and Engineering: R: Reports* **72**, 97 (2011).

## Appendix

### A1. ALUMINA XPS DATA

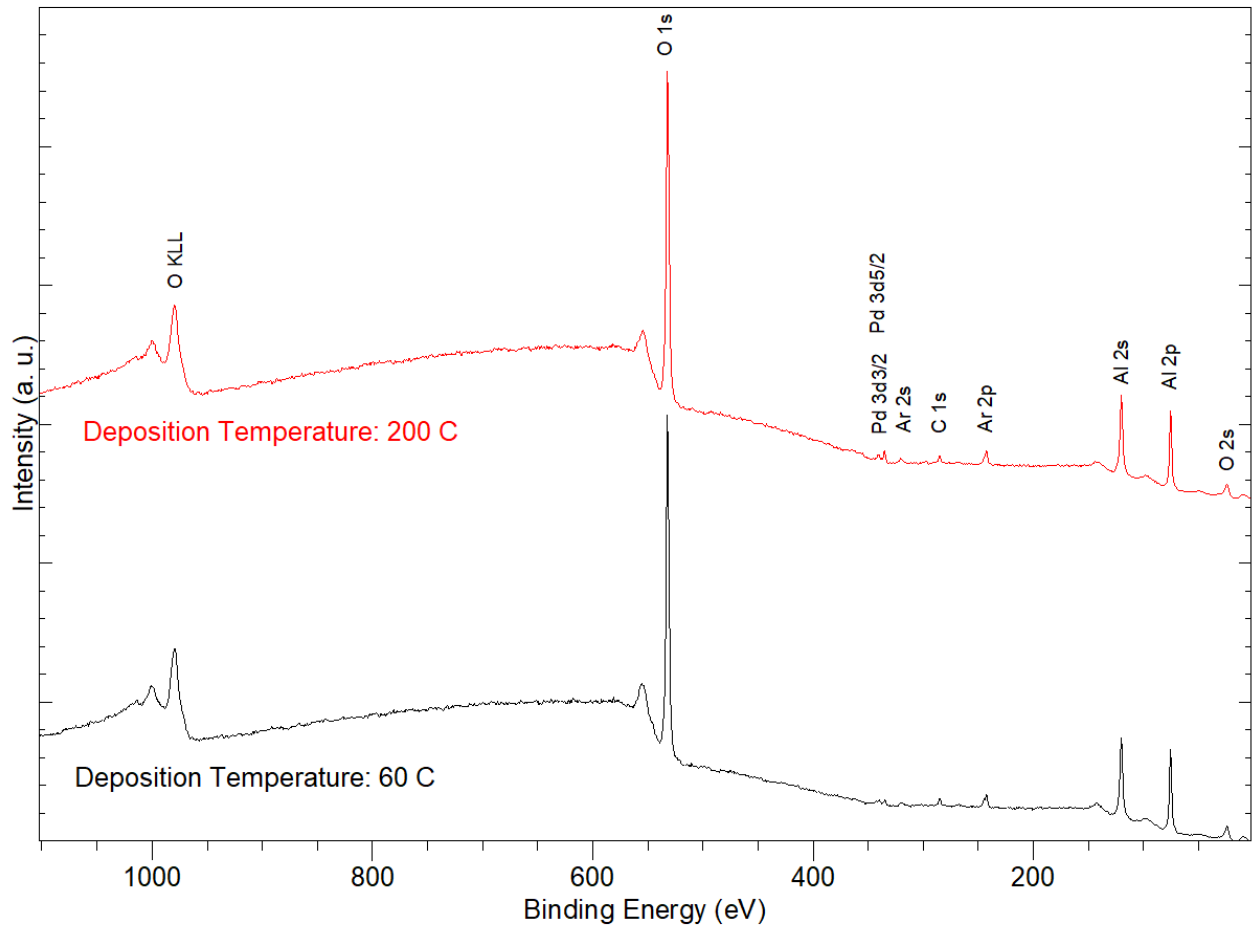


FIG. A1. Survey XPS scans on an alumina film deposited at 200°C (red) and at 60°C (black). Both scans were taken after a nominal 1.5 nm sputter to remove any surface contamination. Palladium peaks arise from the underlying substrate. Argon peaks are remnants of sputtering with an argon ion gun. In the 60°C film, the Al:O:C atomic concentration ratios are 32:64:3. In the 200°C film, the Al:O:C ratios are 34:62:3. While these values have not been calibrated against a sample with known composition and so should not be viewed as quantitatively accurate, the similarity between the two samples suggests almost identical compositions.

### A2. THIN FILMS

In addition to growing thick ( $> 5$  nm) alumina and hafnia films intended to serve as gate dielectrics, we grew thin ( $< 2$  nm) alumina films intended to serve as tunnel barriers. These thin films were grown using the same ALD conditions as the thick films. The films were grown on patterned Pd back contacts, after which Pd top contacts with a Cr sticking layer were added. Pd was chosen to minimize the native oxide formed on the back contact prior to ALD alumina growth. The tunnel junction areas (i.e., lateral overlap between the top and bottom contacts) ranged

from  $8 (\mu\text{m})^2$  to  $500 (\mu\text{m})^2$ . The tunnel resistances of the junctions were characterized by sourcing a DC voltage and measuring the DC current across the tunnel barrier.

We expected that the tunnel resistances would increase exponentially with increasing alumina thickness, and furthermore, that for a given barrier thickness the tunnel conductance would vary linearly with the junction area. The latter implies a constant resistive area (product of junction area and resistance) for a given barrier thickness. Surprisingly, we observed extremely high junction resistances in junctions made with an alumina barrier of four or more ALD cycles, with resistive areas exceeding  $1 \text{ G}\Omega(\mu\text{m})^2$  at room temperature. The resistive areas tended to be higher for junctions of larger area, suggesting that the the measured conduction through the junction is parasitic leakage, not tunnelling. Junctions with zero and two cycle ALD barriers had immeasurably small resistances. We were not able to find an explanation for this behavior, although we found more consistent behavior in barriers grown at high temperature ( $200^\circ\text{C}$  reactor temperature).

### A3. SUGGESTED RECIPES

#### A. Alumina

Heater setpoints:

TMA precursor - unheated  
 Water precursor - unheated  
 Precursor manifold -  $50^\circ \text{C}$   
 Inner chamber heater -  $60^\circ \text{C}$   
 Outer chamber heater -  $60^\circ \text{C}$   
 Exhaust manifold -  $50^\circ \text{C}$   
 Trap -  $50^\circ \text{C}$

Nitrogen flow: 20 sccm

Prepump time: 15 minutes

Repeat for desired number of cycles:

TMA Pulse: 0.015 s  
 TMA Purge: 60 s  
 Water Pulse: 0.015 s  
 Water Purge: 60 s

#### B. Hafnia

Heater setpoints:

TDMA-Hf precursor -  $75^\circ \text{C}$   
 Water precursor - unheated  
 Precursor manifold -  $80^\circ \text{C}$   
 Inner chamber heater -  $85^\circ \text{C}$   
 Outer chamber heater -  $85^\circ \text{C}$   
 Exhaust manifold -  $80^\circ \text{C}$   
 Trap -  $80^\circ \text{C}$

Nitrogen flow: 20 sccm

Prepump time: 15 minutes

Repeat for desired number of cycles:

TDMA-Hf Pulse: 0.3 s  
 TDMA-Hf Exposure: 5 s  
 TDMA-Hf Purge: 40 s  
 Water Pulse: 0.015 s  
 Water Purge: 60 s